Bioactivated and PEG-Protected Circa 2 nm Gold Nanoparticles for in Cell Labelling and Cryo-Electron Microscopy

Nadja Groysbeck, Victor Hanss, Mariel Donzeau, Jean Marc Strub, Sarah Cianferani, Danièle Spehner, Mounib Bahri, Ovidiu Ersen, Mikhail Eltsov, Patrick Schultz, et al.

small methods
www.small-methods.com

Bioactivated and PEG-Protected Circa 2 nm Gold Nanoparticles for in Cell Labelling and Cryo-Electron Microscopy

*Nadja Groysbeck, Victor Hanss, Mariel Donzeau, Jean-Marc Strub, Sarah Cianférani, Danièle Spehner, Mounib Bahri, Ovidiu Ersen, Mikhael Eltsov, Patrick Schultz, and Guy Zuber**

Advances in cryo-electron microscopy (EM) enable imaging of protein assemblies within mammalian cells in a near native state when samples are preserved by cryogenic vitrification. To accompany this progress, specialized EM labelling protocols must be developed. Gold nanoparticles (AuNPs) of 2 nm are synthesized and functionalized to bind selected intracellular targets inside living human cells and to be detected in vitreous sections. As a proof of concept, thioaminobenzoate-, thionitrobenzoate-coordinated gold nanoparticles are functionalized on their surface with SV40 Nuclear Localization Signal (NLS)-containing peptides and 2 kDa polyethyleneglycols (PEG) by thiolate exchange to target the importin-mediated nuclear machinery and facilitate cytosolic diffusion by shielding the AuNP surface from non-specific binding to cell components, respectively. After delivery by electroporation into the cytoplasm of living human cells, the PEG-coated AuNPs diffuse freely in the cytoplasm but do not enter the nucleus. Incorporation of NLS within the PEG coverage promotes a quick nuclear import of the nanoparticles in relation to the density of NLS onto the AuNPs. Cryo-EM of vitreous cell sections demonstrate the presence of 2 nm AuNPs as single entities in the nucleus. Biofunctionalized AuNPs combined with live-cell electroporation procedures are thus potent labeling tools for the identification of macromolecules in cellular cryo-EM.

1. Introduction

Understanding the human cell architecture at the molecular level relies on the availability of advanced microscopes and labeling tools. Developments in cryo-Electron Microscopy (cryo-EM) now enable the recording of cellular images at nanometric resolution detailing multiple molecular components in near native frozen-hydrated conditions.[1] Large protein assemblies such as nuclear pores, ribosomes, microtubules or filaments can be readily visualized, whereas smaller components remain difficult to identify.[2] Gold nanoparticles (AuNPs) with an inner metallic core are popular EM labeling tags, as they efficiently scatter electrons and can be readily functionalized with antibodies to target selected cellular structures/proteins. In most cases, immunogold labeling for cellular EM imaging is performed after resin-embedding on sections of chemically cross-linked cells. However, the visualization of biomolecules in cryo-EM

N. Groysbeck, M. Donzeau, G. Zuber
Université de Strasbourg – CNRS
UMR 7242
Biotechnologie et Signalisation Cellulaire
Boulevard Sebastien Brant, Illkirch F-67400, France
E-mail: zuber@unistra.fr

V. Hanss, D. Spehner, M. Eltsov, P. Schultz
Centre for Integrative Biology (CBI)
Department of Integrated Structural Biology
Institut de Génétique et de Biologie Moléculaire et Cellulaire (IGBMC)
1 rue Laurent Fries, BP10142, Illkirch Cedex F-67404, France

J.-M. Strub, S. Cianférani
Laboratoire de Spectrométrie de Masse BioOrganique
Université de Strasbourg, CNRS, IPHC UMR 7178
Strasbourg F-67000, France

M. Bahri
Albert Crewe Centre
University of Liverpool
4. Waterhouse Building, Block C, 1–3 Brownlow Street, London L69 3GL, UK

O. Ersen
Université de Strasbourg – CNRS
UMR 7504
Institut de Physique et Chimie des Matériaux de Strasbourg (IPCMS)
23 rue de Loess, Strasbourg 67034, France

The ORCID identification number(s) for the author(s) of this article can be found under https://doi.org/10.1002/smtd.202300098

DOI: 10.1002/smtd.202300098

relies on the vitrification of living cells and on maintaining the native cell structure in a frozen-hydrated state throughout the sectioning or milling process up to image acquisition. The strict maintenance of the temperature below -140 °C does not allow for gold labeling following the classical process. This implies that labeling can only be performed before vitrification on unfixed living cells. This constraint has motivated a quest for new tags and methodologies.[3,4] Ideally, the labeling tool must be specific for its target, clearly recognized within the specimen and its use should not denature the specimen. In case intracellular proteins are targeted the probes must be able to freely diffuse in the cytosol.

We previously demonstrated that ultra-small 0.8 nm AuNP-antibodies can be transported into living cells using a cationic lipid formulation and label their target, namely in this case, nuclear RNA polymerase II (PolII).[5] The size of gold nanoparticle attached to the probe was however too small to be revealed effectively by cryo-EM in frozen hydrated cell sections (data not shown). The linkage chemistry was furthermore poorly defined, potentially causing an uncertainty in the distance between the detected gold domain and the targeted epitope. We then screened for gold nanoparticles with increased diameters to facilitate their detection. Mercaptobenzoate-coordinated AuNPs of precise composition[6,7] appear extremely attractive in this regard. They can not only be produced with sizes between 1.2 to 3 nm[8] but also can be functionalized with antibodies via thiolate exchange[9] in aqueous phase. The thiolate-for-thiolate exchange tremendously simplifies the preparation of AuNP-conjugates and opens new ways to design advanced AuNP probes[10] for in situ labeling of supramolecular assemblies and cryo-EM analysis.[11–14] By following the synthesis protocol of thiobenzoate-coordinated gold nanoparticles reported by Levi-Kalisman,[7] we discovered that sodium borohydride reduction of gold(III) chloride in the presence of 5,5'-dithio-bis(2-nitrobenzoic acid) led to 1.4 nm AuNPs covered by a Au-S coordination shell consisting of thioaminobenzoates (TABs) and thionitrobenzoates (TNBs).[15] These mixed TAB-, TNB-coated AuNPs (AuZ) appeared extremely pertinent for bioconjugation purposes and intracytosolic live cell applications. First, the gold nanoparticles reacted well in water near pH 7 with excess thiolated peptides mainly by substitution of TNBs to peptides, producing a gold particle functionalized with 8–9 peptides and the zwitterionic TAB. Second, the organic shell did not dramatically alter HeLa cell viability after cytosolic delivery by electroporation and remained bound to the gold particles.[15] Indeed, the human cells rapidly recovered from the transient electric pulse-mediated permeabilization and withstood the cytoplasmic presence of peptide-functionalized AuNPs. The 1.4 nm AuNP probes coated with the capping peptide of sequence CALNNG[16] could diffuse freely in the cytoplasm and did not accumulate in clusters inside cells as was observed for 2 nm particles delivered by cationic lipid formulation[5] or penetrating peptides.[17] Only SV40 Nuclear Localization Signal (NLS)[18]-conjugated nanoparticles were found to accumulate in the nucleus while Nuclear Export Signal (NES)-conjugated AuNPs were exported from the nucleus.

While these previously published data clearly demonstrated that AuZs are attractive platforms for biofunctionalization and production of AuNPs suitable for delivery into living cells, the 1.4 nm sized-particles still fall short for direct detection with the current electron-dose limitations of cryo-EM for biological specimen.[5,19] It was estimated that AuNPs larger than 2 nm are currently needed for direct detection in cryo-vitrified cell sections.[14] However, this size appears to represent a threshold for protein binding.[20]AuNPs below 2 nm display a strong curvature, and therefore the nanoparticle surface available for binding biomolecules by other means than coordination bonds is limited.[21] With increasing size, the AuNP curvature flattens and the exposed surface presents a larger contact area available for non-specific binding of biomolecules.[22] In the crowded cytosol, weak superficial interactions between AuNPs and the cellular components contribute more to slowing down of the diffusion of the particle than the increase of the hydrodynamic diameter associated with the larger size.[23,24] Hints of the toll taken by non-specific binding of 2 nm AuNPs to cellular components are images showing heterogeneous diffusion pattern and clustering of the nanomaterial in subcellular domains[17,25,26] as well as low specific activity when the AuNPs are equipped with functional elements targeting cytosolic enzymes.[27] Minimizing non-specific binding of molecules using surface-protecting components such as high molecular weight polyethyleneglycol (PEG), which is widely used to decrease non-specific binding of nanomaterial to extracellular constituents[28,29] should enhance binding selectivity and improve the trafficking of the nanomaterial following cytosolic entry.

Here, 2 nm AuZs were synthesized and their surface was functionalized with SV40 NLS peptides and surface capping agents, by thiolate to thiolate exchange. Amongst the various tested capping elements, the 2 kDa polyethyleneglycols (PEG) was the most effective and was coordinated to the AuNP surface in combination with a NLS peptide at different proportion. After characterization, the functionalized AuNPs were first incubated with living HeLa cells to assay cytotoxicity and non-specific cellular penetration and distribution. The gold nanoparticles were then delivered into the cytosol of living cells using an electroporation procedure and cell viability, probe distribution, and nuclear import efficiency were assayed. The PEG-,NLS-coated AuNP (AuPEGNLS) with an equal amount of NLS and PEG conjugated to the AuNP surface showed weak non-specific binding to general cellular components while performing highly efficient NLS-mediated nuclear import. We further demonstrate that the 2 nm AuPEGNLSs after electroporation are directly detected within the nucleus in unstained vitreous cell sections by cryo-EM.

2. Results and Discussion

2.1. Synthesis and Characterization

The AuZs were synthesized in acetonitrile/water mixture[30] by sodium borohydride reduction of auric chloride in the presence of Ellman's reagent.[31] Characterization by gel electrophoresis, transmission electron microscopy, and MALDI-TOF revealed a monodisperse solution of particles with an average diameter of 2.02 nm (SD 0.21, n = 105) and a molecular mass of 60 kDa (Supporting InformationFigure S1, Supporting Information). The gold particles were then reacted with increasing molar ratios of the NLS peptide whose sequence (CALNNGAGP-KKKRKVED) contains the classical SV40 NLS[18] and with

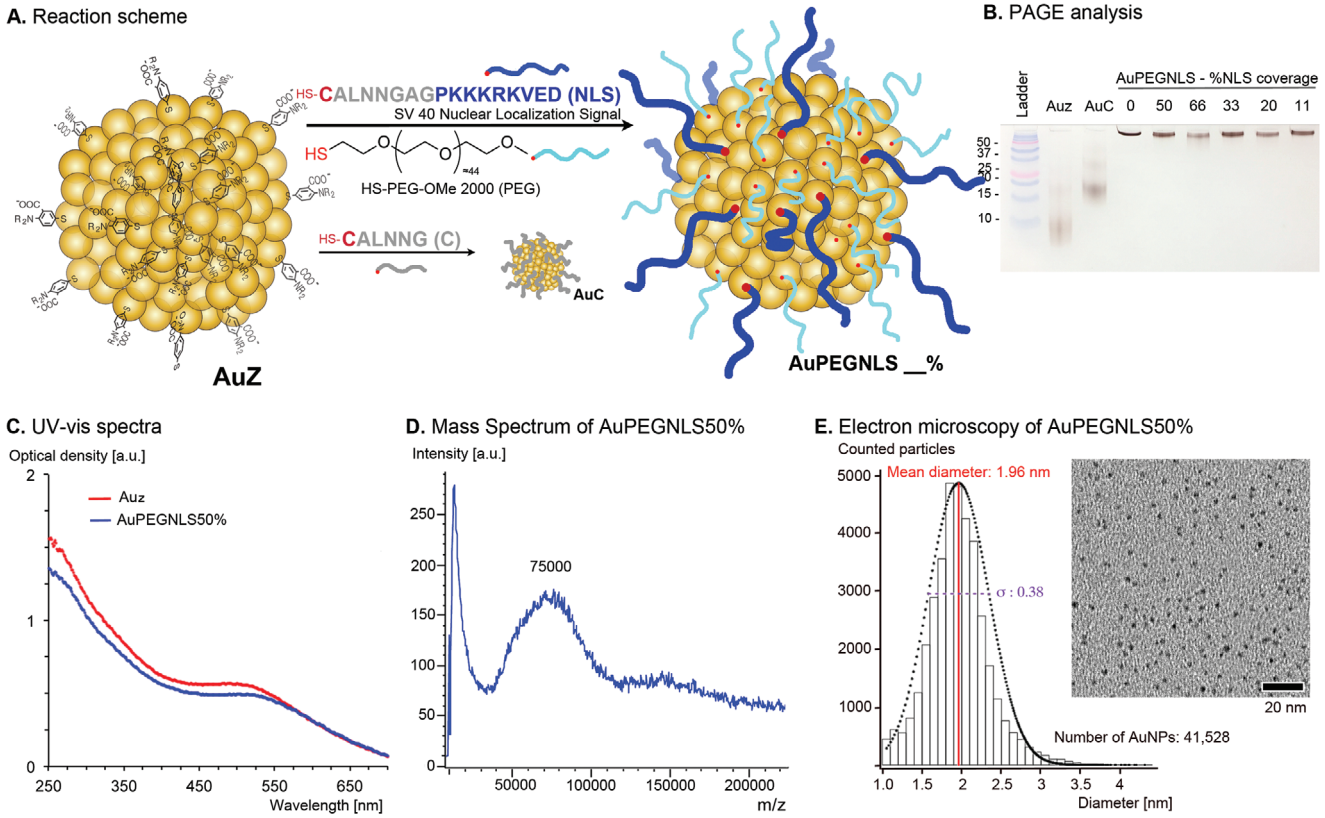

Figure 1. Preparation and characterization of polyethyleneglycol -, Nuclear Localization Signal peptide - decorated AuNPs. A)Illustration of the AuNPs and synthesis scheme. The percentage refers to the relative amounts of NLS peptide to total (PEG + NLS) thiolates. As a control, the AuZwas also reacted with CALNNG forming the AuC nanoparticles. B)Polyacrylamide gel electrophoresis analysis of the starting AuZ, purified AuC, and AuPEGNLS at the indicated NLS proportion. C)UV–vis spectrometry of AuZ (in red) and AuPEGNLS50% (in blue). D)MALTI-TOF Mass spectrum of the AuPEGNLS50%. E)Electron microscopy image of AuPEGNLS50% and population analysis of the gold particle diameter.

a previously described gold particle capping peptide whose sequence (CALNNG)[16] carries a reactive Cysteine at its N-terminus. The degree of ligand exchange on the particle surface was analyzed by monitoring stably bound NLS peptides to AuNPs by gel electrophoresis (Figure S2, Supporting Information). Substitution of AuZ-coordinated thiobenzoates by the NLS peptide expectedly increased when the peptide/AuZ ratios rose from 4 to 30. Excess NLS-coating of the 2 nm AuZ particles led to precipitation, which was not observed with the 1.4 nm AuZ.[15] This undesired precipitation is likely a consequence of the surface area of a 2 nm particle (calculated area of 12.6 nm^2) that is twice the one of a 1.4 nm particle (area of 6.15 nm^2) and prompted us to complement the conjugation of the bioactive NLS with a surface protecting element. Thiolated reagents ensuring effective protection for gold surfaces from associating with biomolecules are scarce. Glutathione[17,27] and 0.6 kDa thiolated PEG[32] were first tested as passivation agents for AuZ. Unfortunately, mixing the glutathione or the 0.6 kDa thiolated PEG with AuZ led to precipitates that were uneasy to re-suspend in aqueous solutions near pH 7.0. In contrast, addition of CALNNG peptide[16] or thiolated 2 kDa PEG to AuZ maintained the gold particles in suspension and formed the AuC and AuPEG components, respectively, via the expected thiolate to thiolate exchange. The NLS peptide was incorporated in the AuPEG shell at relative thiolate amounts of 11, 20, 33, 50, and 66%, thus yielding the AuPEGNLSs with the indicated NLS% (**Figure 1**A).

All functionalized AuNPs were purified by gel filtration chromatography, concentrated by ultracentrifugation, and behaved as stable colloids. Their electrophoretic mobility was different than the starting AuZ (Figure 1B). Regardless of the NLS proportion, the AuPEGNLS did not enter the gel, indicating that the thiolated 2 kDa PEG are coordinated onto the gold surface in a high density. The intensity of Coomassie blue staining of each AuNP grew as a function of increasing NLS proportion, indicating that the number of NLS peptides conjugated per AuNP increased as well (Figure S3, Supporting Information). All AuPEGNLSs show UV–vis spectrum similar to that of AuZ with a similar absorption shoulder at 520 nm (Figure 1C; Figure S4, Supporting Information). The concentration of the gold nanoparticles was determined by spectrometry measurement at 520 nm using an absorption coefficient of 510 000 M^{-1} cm^{-1} according to the formula proposed by Liu et al.[33] The MALDI-TOF Mass spectrum of the AuPEGNLS50% (Figure 1D) was representative of all the other AuPEGNLS spectra (Figures S5–S10, Supporting Information). A broad distribution of masses centered at ≈75 kDa was observed as compared to 60 kDa for AuZ. The roughly 15 kDa difference in mass likely measures the exchange of about ten 0.2 kDa TNBs to ten 2 kDa PEGs and 1.8 kDa NLSs. This

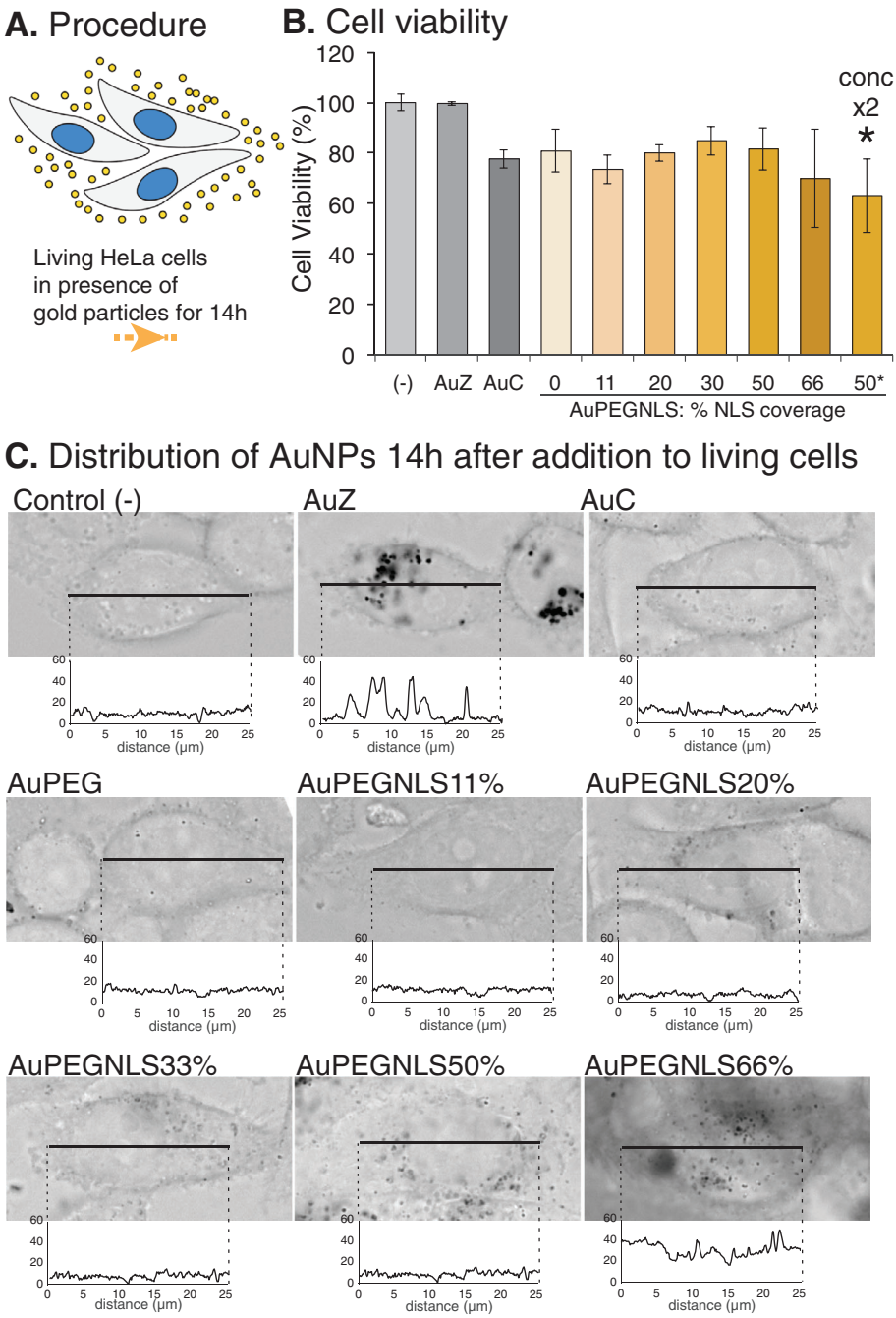

Figure 2. Analysis of cell viability and gold particle distribution following their incubation with HeLa cells for 14 h as indicated. A)Freshly trypsinized HeLa cells (10^5 cells/10 µL PBS) alone or with 5 µM of each AuNP (10 µM AuPEGNLS50% in the * marked condition), were incubated for 10 min before dilution in 1 mL cell culture medium containing 10% serum. Cells were then dispatched in plates for cell culture at 37 °C during 14 h (final concentration of AuNPs after dilution: 0.5 µM (1 µM for*). B)The cell viability as estimated with the MTT assay.[34] Values are averages and standard deviations of quintuplicates. C)Light microscopy images and distribution profiles of AuNPs along the indicated lines. Cells were fixed with 2% glutaraldehyde, permeabilized with 0.1% saponin and the gold particles were silver-enhanced for detection.

substitution number suggests that the AuPEGNLS50% is grafted with 5 PEGs, 5 NLSs and residual TABs and TNBs. Electron micrographs showed evenly distributed individual particles on the carbon film. Statistical analysis of 41528 imaged particles resulted in an average diameter of 1.96 nm and a standard deviation of 0.38 nm.

2.2. Distribution Profiles Upon Addition to Living Cells

The above-characterized AuNPs were then incubated with living HeLa cells for 14 h in order to analyze their cytotoxicity (**Figure 2**). HeLa cells were freshly trypsinized to detach them from the Petri dishes, concentrated to obtain 10^5 cells in 10 µL of PBS and mixed

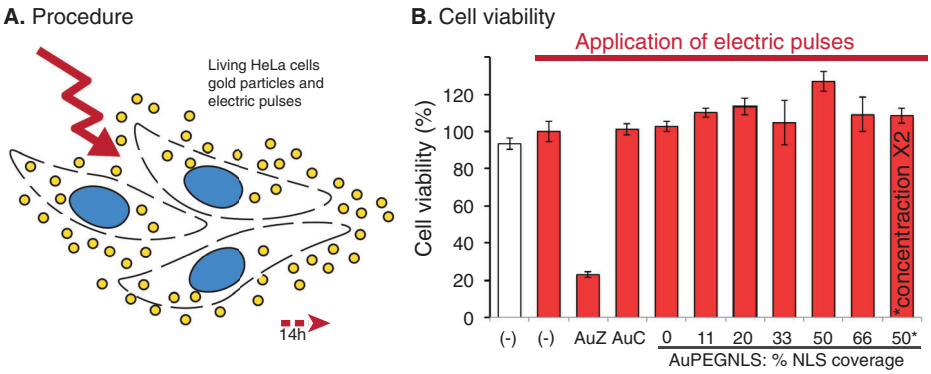

Figure 3. Analysis of cell viability following electroporation of HeLa cells incubated with the indicated gold particles. A)Freshly trypsinized HeLa cells (10^5 cells/10 µL PBS) alone (-) or with 5 µM of each AuNP (10 µM AuPEGNLS50% in the * marked condition) were subjected to 3 electric pulses of 10 ms at 517 V cm^{-1}. Cell suspensions were diluted in 1 mL cell culture medium containing 10% serum and AuNPs remaining in solution were separated from cells by centrifugation. The cell pellets were then re-suspended in cell culture medium for culture during 14 h. B)Cell viability was estimated with the MTT assay.[34] Values are averages and standard deviations of quintuplicates.

with 5 µM of each AuNP. After 10 min of incubation, the cells were diluted in cell medium containing serum and incubated for growth before analysis of cell viability and AuNP localization 14 h latter. HeLa cells with proteolytically removed adhesion receptors (e.g., trypsin cleaves superficial proteins involved in adhesion) but with native plasma membranes tolerate well the presence of the different AuNPs as evidenced by the recovery of <70% viable adhered cells relative to control even in the presence of 1 µM AuPEGNLS50%. (Figure 2B). The localization of the AuNPs was then monitored. The cell culture media containing unbound gold particles were removed. The cells were washed with PBS, fixed with glutaraldehyde and subjected to silver-enhancement (Figure 2C).

The AuZ particles gave rise to intense cytoplasmic aggregates likely because of their ability to react with thiols on the cell surface and their uptake into vesicular compartments. The AuC, AuPEG, AuPEGNLS 11% and AuPEGNLS 22% were barely seen on the cell surface and even less so within cells suggesting that they do not significantly bind to the plasma membrane (Figure 2C). Accumulation into discrete dots at the plasma membrane and within the cytoplasm was observed for AuPEGNLS33%, 50%, and 66%. The staining intensity increased as a function of the NLS content in the AuPEGNLS shell. The AuPEGNLS66% even strongly adhered to the glass support. The electrostatic associations between cationic NLSs and anionic proteoglycans present on the cell surface and the continuous recycling of the plasma membrane into intracellular vesicles may account for the observed gold particle distribution.[35] Regardless of the coverage, the AuNPs did not accumulate in the nucleus and did not diffuse into the cytosol. Intravesicular entrapment of gold particles without cytosolic release upon addition to living cells is expected[15,36] since the rupture of the endosomal bilayer, although possible,[37,38] remains a rare event.

2.3. Distribution Profiles after Entry into the Cytoplasm of Living Cells

The cytotoxicity and distribution of the AuNPs within living cells was investigated after having delivered the probe using a commercially available electroporation device[39] and electric pulses that were previously optimized for antibody transduction[15,40] (**Figure 3** and **Figure 4**). AuNPs at the indicated final concentrations were incubated with freshly suspended HeLa cells in PBS. The solutions were then subjected to 3 electric pulses of 10 ms at 517 V cm^{-1} to create transient holes in the plasma membrane and hence cytosolic entry of the extracellular applied components. After the electric pulses, excess AuNPs in solution were removed and the electroporated cells were cultivated for 14 h before testing the recovery of cell viability and the distribution of AuNPs as described above. The cell viability was compared to cells in PBS without application of electric pulses or to cells in PBS treated with electric pulses. Except for AuZ, application of the 3 electric pulses and presence of AuNPs did not affect cell viability (Figure 3B). The highly thiol-reactive AuZ may trap essential cellular components and induce cell death.

The cellular distribution of the electroporated functionalized AuNPs (Figure 4A) was remarkably different than the ones reported in Figure 2C, confirming that the gold particles entered the cell and that their intracellular location was determined by the functions introduced on their outer shell. The non-functionalized AuZ did not diffuse freely but rather accumulated in cell membrane-bound aggregates or within intracellular vesicles.

The mobility of the thiol-reactive AuZ was probably hampered by its ability to react with thiolate-containing cell components and hence be trapped there. The internalized AuCs appeared to distribute throughout the cell, including to some extent in the nucleus. Aggregate formation was also clearly observed in perinuclear vesicles resembling lysosomal compartments. The AuPEGs appeared homogeneously dispersed in the cytoplasm and were mostly excluded from the cell nuclei in agreement with the fact that nuclear import of inert material larger than 5 nm in diameter is severely restricted by the nuclear pore complex.[41,42] In fact, the 2 kDa PEG molecules surrounding the 2 nm gold particles have a contour length of 12.5 nm which increases the maximal diameter of the particles to 27 nm. In contrast to the AuPEG, the NLS functionalized AuPEGNLSs accumulated in the nuclei and preferably in the nucleoplasm rather than in nucleoli. To analyze the nuclear accumulation of AuNPs, we plotted the

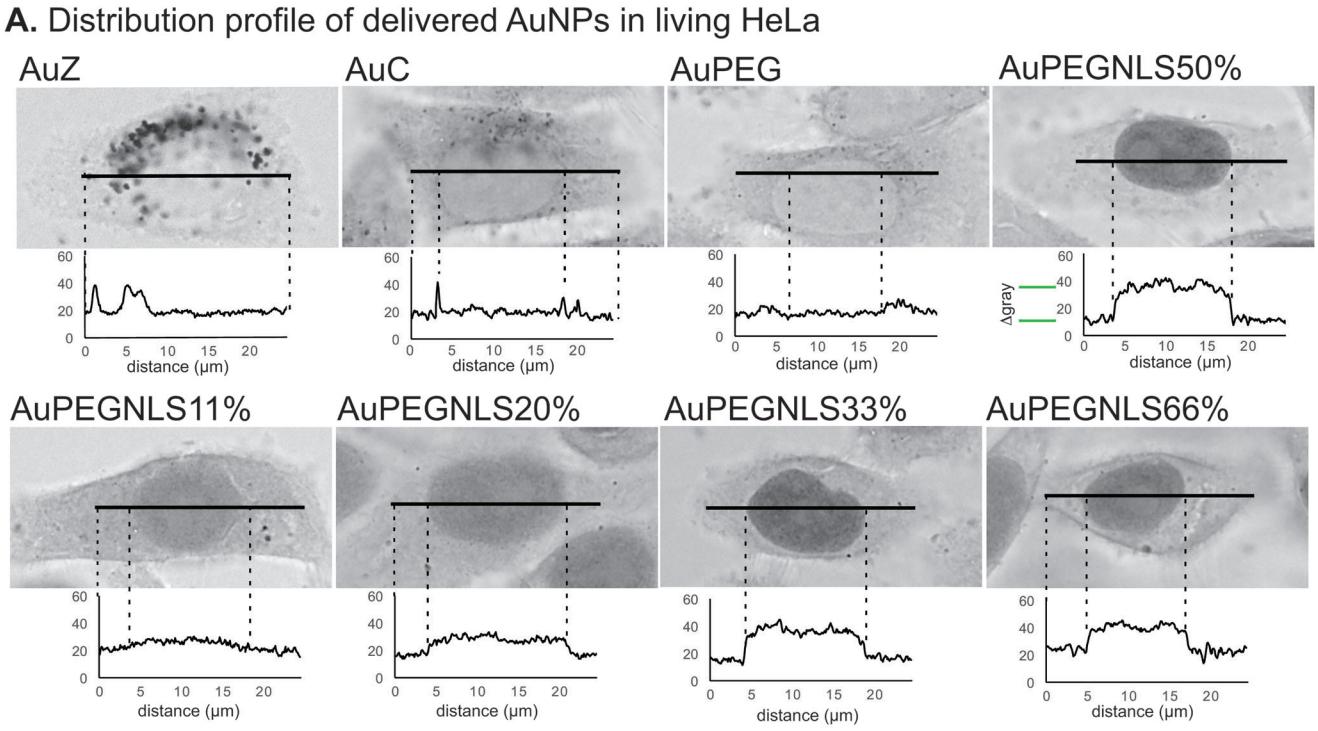

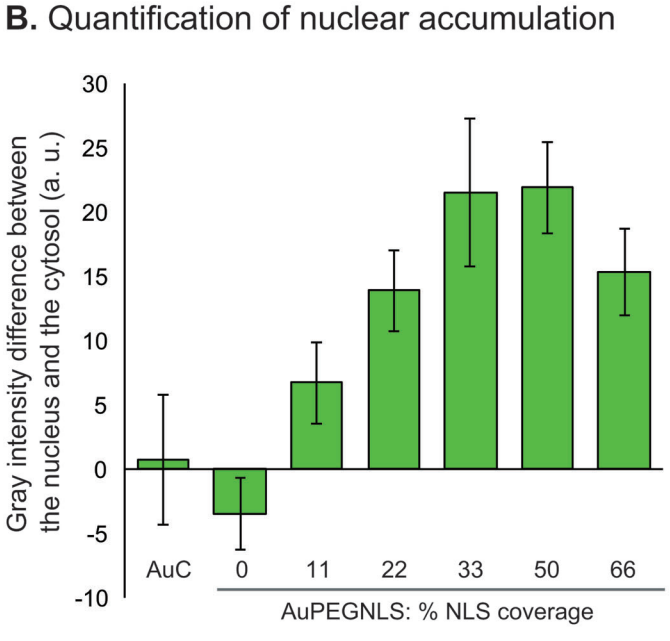

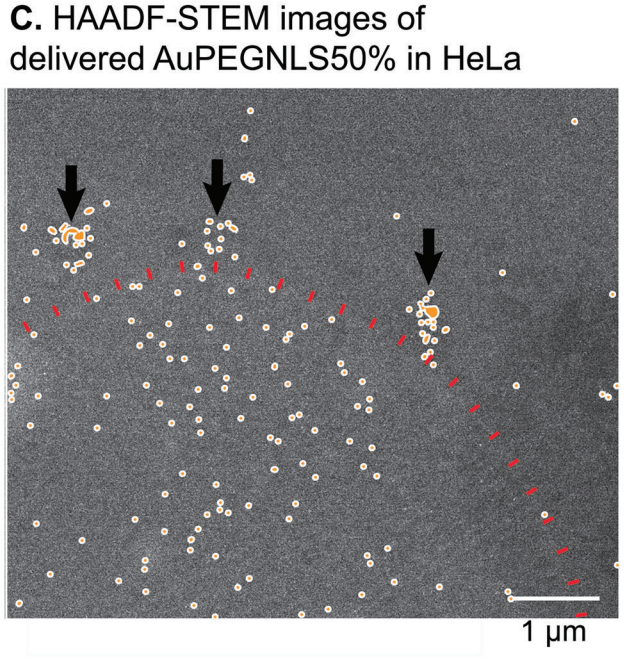

Figure 4. Intracellular AuNP distribution after AuNP delivery by electroporation. A)Light microscopy images and distribution profiles of the indicated AuNPs 14 h after transient plasma membrane permeabilization, and subsequently silver enhanced cells. The graphs represent intensity plots along the indicated lines and reveal the AuNP distribution. B)Quantification of nuclear accumulation. Differences in staining between the nucleus and the cytosol were measured using gray plots from silver-enhanced cell images containing the indicated delivered AuNPs. Values are averages and standard deviations of 14 measures. C)HAADF-STEM images of a HeLa section containing delivered AuPEGNLS50%. After delivery and cell culture, the cells were fixed, the AuNPs were enhanced with silver and the specimen embedded in resin for room temperature electron microscopy imaging. For sake of clarity, the nuclear envelope (dotted red line) and the barely visible AuNPs (orange dots) were marked. The 3 black arrows point to AuNPs entrapped in cytoplasmic vesicles.

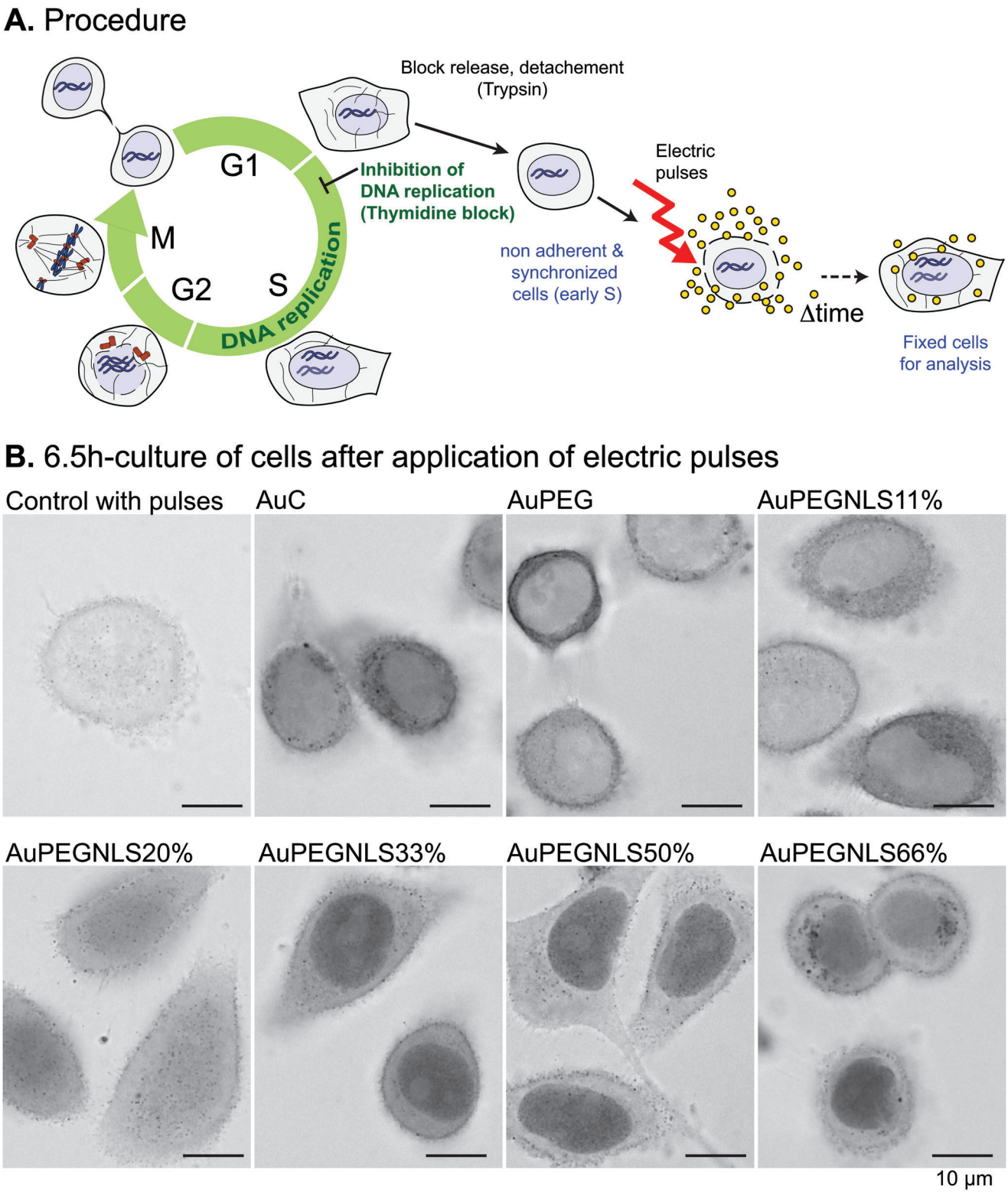

Figure 5. Analysis of cell content 6.5 h after application of electric pulses to HeLa cells synchronized to be in early S phase and incubated with the indicated AuNPs. A)Scheme of the procedure. B)Distribution of the indicated gold nanoparticles in synchronized HeLa cells 6.5 h after release of the inhibition of DNA replication and application of the electric pulses (3 pulses of 10 ms at 517 V cm^{-1}). The cells were fixed with 2% glutaraldehyde, permeabilized with 0.1% saponin and the gold particles were enhanced with silver for detection by light microscopy.

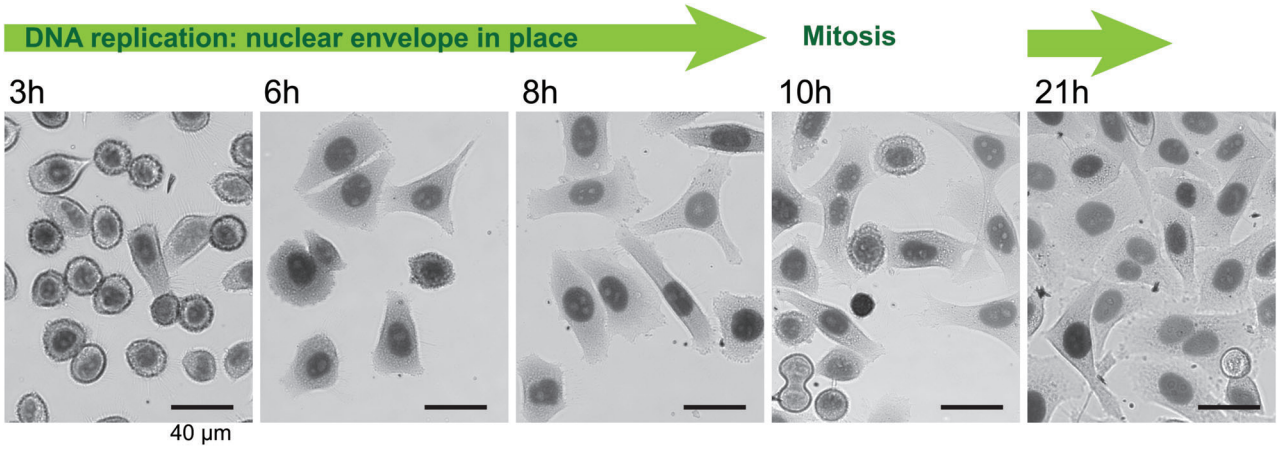

Figure 6. Light microscopy images of HeLa cells containing AuPEGNLS50% at different time points after electroporation and release of the inhibition of DNA replication. The cells were fixed with 2% glutaraldehyde, permeabilized with 0.1% saponin and the gold particles were silver-enhanced for detection by light microscopy.

intensity profile along a line crossing cytoplasmic and nuclear regions of the silver enhanced cells (Plots in Figure 4A). The intensity ratios between the average nuclear and cytoplasmic values were then calculated to quantify the nuclear accumulation (Figure 4B). The nuclear accumulation of the AuPEGNLSs consistently increased with the NLS density indicating that nuclear import depends on the NLS coverage. The maximum import was reached with 33% and 50% NLS coverage and was found to decrease for the 66% NLS coverage. This may be related to the intracellular aggregation observed in the control experiments with AuPEGNLS66% nanoparticles. Although the import efficiency was comparable for AuNPs with 33 and 50% coverage, the lower standard deviation of AuPEGNLS50% prompted us to employ them to prepare samples for EM observation. A first HAADF-STEM imaging of the AUPEGNLS50% particles delivered into living HeLa cells was performed at room temperature after silver enhancement and resin embedding (Figure 4C). With the exception of AuNPs entrapped within vesicular compartments at the vicinity of the nuclear envelope (black arrows), only a few particles were detected in the cytoplasm while the vast majority of AuNPs were found in the nucleus as single particles.

2.4. Distribution Profiles after Entry into the Cytoplasm of Synchronized Cells

To further demonstrate without ambiguity that the NLS-functionalized AuPEGs are shuttled into the nucleus via the nuclear pores using the importin pathway and not trapped during mitosis,[43] DNA replication was inhibited with a double thymidine block to hold the cells in early S phase (**Figure 5**A).[44] The synchronized cells were then released from the DNA synthesis inhibition just before the electroporation procedure and the AuNP distribution was analyzed after growing the cells for 6.5 h (Figure 5B). At the arrest time, most synchronized cells remained in S phase and did not undergo nuclear envelope breakdown and mitosis. The distribution profiles of the different AuNPs were extremely similar to those obtained 14 h after cytosolic delivery and without thymidine block (Figure 4). The AuPEG, AuC, and AuPEGNLS11% were mainly distributed in the cytosol with clear contact to the cytosolic face of the nuclear envelope. The AuPEGNLS20% entered the nucleus albeit poorly. Darker grains near the nuclear envelope were observed, suggesting that these gold particles, 6.5 h after entry were still proceeding for association to importin and for passage across the gel protecting the hole of the nuclear pores.[41,45] The AuPEGNLS33% and 50% with the highest NLS density were efficiently imported into the nucleus with apparently few nanoparticles remaining in the cytosol. The AuPEGNLS66% also accumulated in the nucleus but was also detected in perinuclear compartments resembling lysosomes, likely because the number of NLS peptides attached to these gold particles favor unspecific binding to the external surface of the plasma membrane and engulfment in intracellular vesicles via the plasma membrane recycling process.

The living cells containing AuPEGNLS50% were then grown for 3,6,8,10, and 21 h in order to analyze the dynamics of intracellular AuNP distribution before and after mitosis (**Figure 6**).

The HeLa cells slowly formed adhesion contacts onto the cell culture dish and the AuPEGNLS50% readily accumulated in the cell nuclei following the electric pulses. Robust and near complete nuclear import was observed during the S phase when the nuclear envelope remains intact (3, 6, and 8 h time points). The cells then entered and exited mitosis without major perturbation, confirming that HeLa cells withstand the transient electric pulse- mediated permeabilization and the intracellular presence of AuPEGNLS50%. The fast nuclear import of the NLS-equipped AuNPs following delivery parallels the behavior of NLS-containing proteins and confirms the relative inertness of the probes.[42] Of note, 2 nm AuPEGNLSs were also efficiently shuttled into the nuclei of U2OS following electroporation without marked cytotoxicity (Figure S11, Supporting Information), indicating that this protocol is applicable to other human cell lines.

2.5. Cryo-EM Imaging

In a final experiment, we investigated whether the 2 nm gold particles could be detected without silver enhancement within the

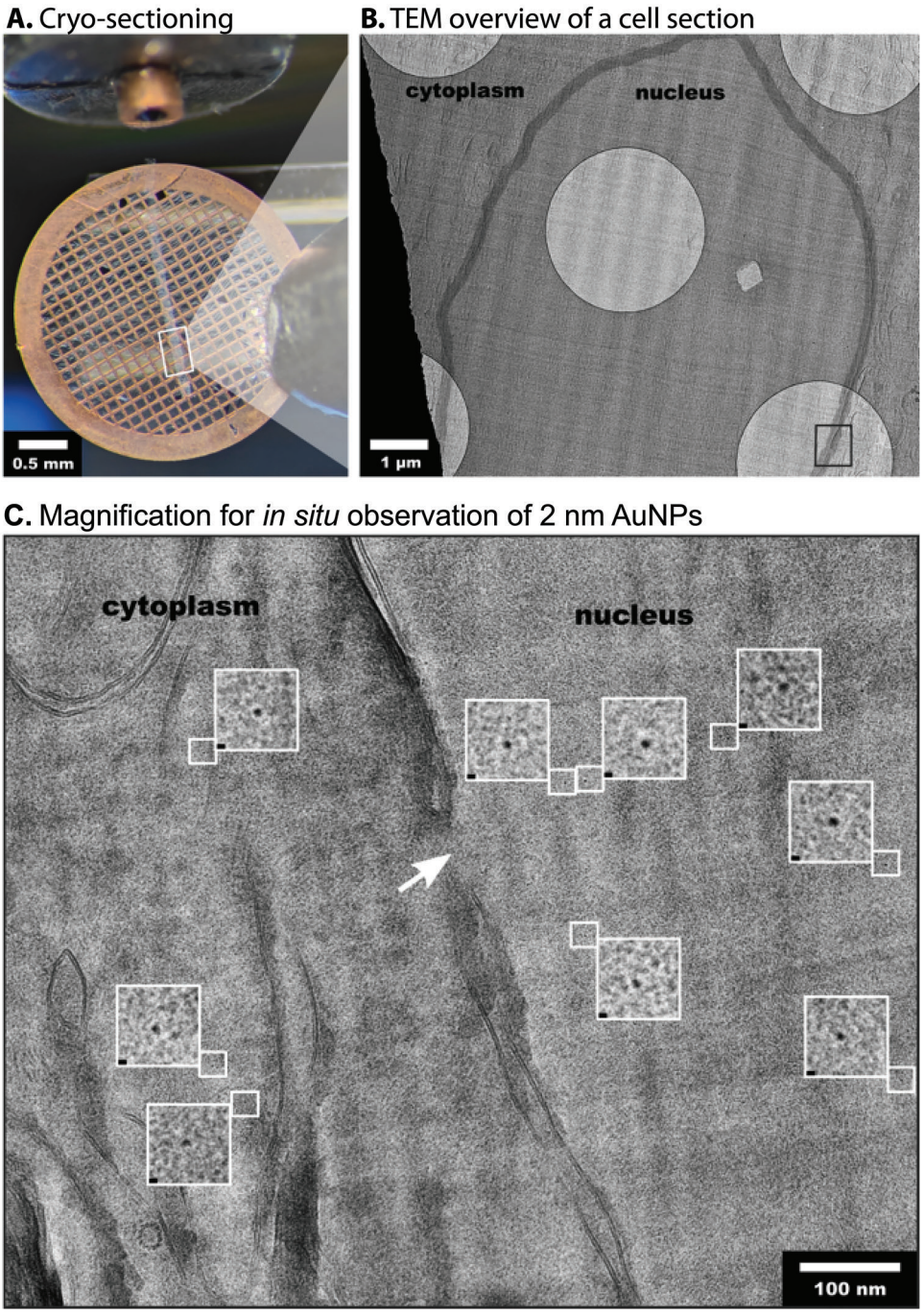

Figure 7. Cryo-EM workflow of high-pressure frozen HeLa cells electroporated with AuNLSPEG50%. A)The vitrified specimen was sectioned in cryogenic conditions using a cryo-ultramicrotome. The resulting translucent ribbon was deposited on a copper grid covered with a perforated carbon film and observed in cryo-Electron Microscopy. B)Cryo-EM micrograph showing a portion of cell centered on its nucleus where the nuclear envelope is highlighted. C)Magnified area around the nuclear envelope (black rectangle in (B)) showing subcellular structures including a nuclear pore (white arrow) separating the cytoplasm (left side) from the nucleus (right side). Gold particles in small boxesare enlarged 4 times (large inserts with 2nm black scale bars on bottom left corners) for better visibility.

unstained and fully hydrated cell nucleus by Cryo-Electron Microscopy Of Vitreous Sections (CEMOVIS).[1,46] The functionalized AuPEGNLS50% were delivered into the cytoplasm of living cells by electroporation and the cells were grown for 18 h before vitrification by high pressure freezing. Ribbons of vitreous cell sections were obtained using a cryo-ultramicrotome, collected on EM grids and imaged in cryo-EM (**Figure 7**).

At low magnification (Figure 7B), the cryo-TEM image showed a cell section centered on the nucleus and surrounded by the cytoplasm. The light grey holes correspond to transmitted

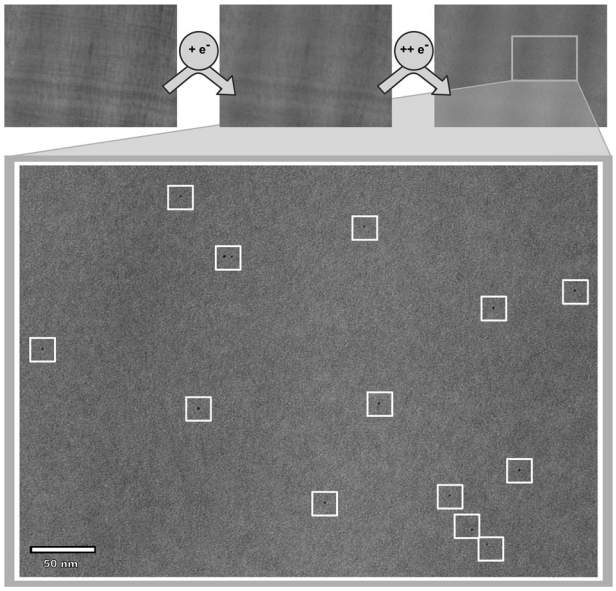

Figure 8. Identification of gold particles in the nucleoplasm after radiolysis of biological structures by irradiation with a high electron dose. The structural aspect of the vitreous section gradually changes after irradiation by 20, 80, 120e^{-} $Å^{-2}$ (upper row). Gold particles are the only high contrast structural features remaining after high dose irradiation.

information through the specimen only whereas the dark grey corresponds to an image of the specimen plus the carbon film. Magnification into a hole crossed by the nuclear envelope was performed to observe a nuclear pore and electron dense dot-like structures compatible with the size of AuNPs (Figure 7C). The contrast of these single dots was higher than for subcellular structures such as biological membranes but expectedly faint. To verify that these densities indeed represent the AuNPs, we applied a higher electron dose to the sections (120 e $Å^{-2}$) than one normally used for imaging (10 e $Å^{-2}$) (**Figure 8**). This treatment results in radiolysis of biological molecules but not of inorganic materials. The 2 nm-sized densities remained after radiolysis and became even more contrasted, thus confirming the presence and the ability to detect 2 nm gold particles in two-dimensional cryo-EM images of a crowded cellular section. All detected particles appeared as single and non-aggregated entities. Furthermore, and in agreement with our light microscopy results, a higher concentration of AuNPs was observed within the cell nucleus.

3. Conclusion

To use functionalized gold nanoparticles for intracellular labeling and cryo-EM observations, the penetration and diffusion abilities of the probe must be worked out in concert. We report the optimization of the surface coverage of 2 nm TAB-, TNB-protected AuNPs with bioactive NLS ligands and surface-protecting PEG in a controlled way through thiolate exchange. We then delivered these AuNPs into living cells by electroporation. The PEG coverage considerably limited intracytosolic clustering and non-specific adherence to cellular components ensuring a robust SV40 NLS targeting of the nuclear import pathway and the shuttling of the gold particle into the nucleus. Direct detection of individual 2 nm AuNPs within the nuclei of cryo-fixed cells, proves that 2 nm-sized AuNPs provide sufficient contrast to be detected even when embedded within the crowded environment of the cell nucleus. We strongly believe that this identified size range and PEG coverage opens multiple possibilities to generate specific gold immunolabelling tools for deciphering the distribution of intracellular components within living cells after delivery using a convenient electroporation procedure.

4. Experimental Section

General: Materials and additional protocols were described in the supporting information. The staining profile was measured using Image J[47] by plotting the gray value profiles underneath the indicated lines spanning the cell nuclei.

Synthesis of AuPEGNLS50%: A solution of 10 µM 2 nm AuZ[30] (90 µL, 0.9 nmol) was mixed with 1 M HEPES pH 7.4 (10 µL) and then rapidly added to a freshly mixed solution containing 10 mM CALNNGAGPKKKRKVED peptide (4 µL, 40 nmol), 5 mM tris(-2-carboxyethyl)phosphine, pH 7.4 (8 µL, 40 nmol), and 20 mM thiolated PEG 2000 (PEGSH; 2 µL, 40 nmol) into a 0.5 mL polypropylene tube. The mixture was incubated at room temperature for 16 h. The crude mixture was then purified by size exclusion chromatography (Sephadex G-25, PBS as elution buffer) followed by 7 cycles of ultrafiltration (dilution in sterile PBS) using a 0.5 mL Microcon® centrifugal filter device with 30 kDa cut-off (Merck, Molsheim). At the end of the process, a 60 µL volume was recovered containing AuPEGNLS50% at an estimated concentration of 12 µM (0.72 nmol; 80% recovery yield). The other AuPEGNLSs at different NLS percentage were prepared using the same procedure and an identical [NLS thiolate peptide+PEGSH]/AuZ ratio of 80/0.9. After ultracentrifugation, the AuPEGNLS50% was obtained at a concentration of 30 µM.

Synchronization of HeLa Cells: Adherent HeLa cells were synchronized using a double thymidine block method.[44] Thymidine (Sigma) was added to the cell culture media at a final concentration of 2 mM from a 100 mM stock solution in water. The cells were incubated for 16 h at 37 °C, after which the culture media was removed, the cells were washed three times with sterile PBS and normal growth medium was added again. Following 8 h at 37 °C, thymidine was added a second time at a final concentration of 2 mM for additional 16 h.

Electroporation Protocol: Transient permeabilization of the plasma membrane of living cells was conducted using the Neon^{R} transfection system[39] with three 10 ms pulses at 517 V cm^{-1}.[40] For a final electroporation volume of 10 µL, HeLa cells (2×10^5 cells in 10 µL of the Neon Buffer R) were mixed with each functionalized gold nanoparticle (50 pmol at 5 µL of a 10 µM solution in PBS). After electroporation, the cells were diluted into prewarmed cell culture medium with 10% fetal calf serum (FCS) but without antibiotics (1 mL). The cells were pelleted by gentle centrifugation (100 RCF), suspended into warmed cell culture medium with 10%FCS without antibiotics (0.5 mL) and added into 24-well plates containing 13 mm diameter cover glass or into 35 mm Ibidi dishes (Ibidi: ref 80 136 or 80 156). Plates or dishes were then placed inside a cell culture incubator at 37 °C, 5% CO_2 for cell adherence and growth.

Cell Viability Assay: The assay was done according to a published procedure.[34] Electroporated cells and untreated cells were diluted in 0.5 mL cell culture medium and divided in fractions of 100 µL in a 96-well plate. The cells were incubated at 37 °C, 5% CO_2, for 24 h before addition of thiazolyl blue tetrazolium bromide solution in PBS (10 µL of a 5 mg mL^{-1}) for quantification of the released formazan.

Cellular Specimen preparation for Light Microscopy: The treated cells, grown on cover glasses or Ibidi dishes, were washed twice in PBS (2×1 mL). The cells were then fixed with 2.0% glutaraldehyde in 100 mM Sorenson's buffer (1 mL) for 4 h. After removal of the fixative and 3 PBS washes (1 mL), unreacted aldehydes were blocked by incubation with a 100 mM Sorenson's buffer, pH 7.4 containing 50 mM glycine (1 mL, 20 min). The plasma membrane was permeabilized using 0.1 M Sorenson's buffer pH 7.4 containing 0.1% (w/v) saponin (1 mL, 15 min)

before proceeding for silver-mediated amplification of the gold particles according to a modified Danscher protocol using silver acetate and propyl gallate.[48] Briefly, the phosphate-buffered solution was replaced by a 0.1 M citrate solution, pH 6.7 containing 2% sucrose (5 washes). Silver-enhancement of the specimen was then done in a dark room for 8 min using a freshly prepared 6 mM silver acetate solution in 0.16 M sodium citrate, pH 6.7 containing 2 mM propyl gallate and 20% gum arabic. The silver-mediated AuNP staining solution was then removed from the specimens with extensive washes using 0.16 M sodium citrate solution, pH 6.7 (1 mL) and then PBS (0.5 mL). The specimens on the cover glasses were finally mounted onto 3×1 inch microscope slides (knittelglass.com) using Fluoromount-G (Southern Biotech, Ref. 0100–01, batch I2819-WC79B). Observations were carried with Leica DM5500B microscope equipped with HCX PL Apo 63×1.40 oil PH3CS objective and a Leica DFC350FX camera. When cells were grown on 35 mm Ibidi dishes, the observations were carried out with an Olympus IX83 equipped with LUCPLFLN 40×0.6 objective and a CMOS Hamamatsu Orca Fusion camera (C144440-20UP) directly after the silver-enhanced procedure.

Supporting Information

Supporting Information is available from the Wiley Online Library or from the author.

Acknowledgements

This research was supported by the ITI Innovec (IdEx (ANR-10-IDEX-0002), SFRI (ANR-20-SFRI-0012)), the French Infrastructure for Integrated Structural Biology (FRISBI ANR-10-INBS-05), and the ITMO Cancer (ColorME, 22P096-00). N.G. received a Ph.D. fellowship from the IdEX Unistra (Université de Strasbourg and Investissements d'Avenir). V.H. received a fellowship from the CNRS. Robert Drillien styleedited the text.

Conflict of Interest

The authors declare no conflict of interest.

Data Availability Statement

The data that support the findings of this study are available in the supplementary material of this article.

Keywords

bioconjugation, electroporation, gold labeling, gold particles, nuclear import, transduction

Received: February 10, 2023
Revised: March 9, 2023
Published online:

[1] A. Al-Amoudi, J.-J. Chang, A. Leforestier, A. McDowall, L. M. Salamin, L. P. O. Norlén, K. Richter, N. S. Blanc, D. Studer, J. Dubochet, *EMBO J.* **2004**, *23*, 3583.
[2] J. Mahamid, S. Pfeffer, M. Schaffer, E. Villa, R. Danev, L. K. Cuellar, F. Förster, A. A. Hyman, J. M. Plitzko, W. Baumeister, *Science* **2016**, *351*, 969.
[3] Z. Jiang, X. Jin, Y. Li, S. Liu, X.-M. Liu, Y.-Y. Wang, P. Zhao, X. Cai, Y. Liu, Y. Tang, X. Sun, Y. Liu, Y. Hu, M. Li, G. Cai, X. Qi, S. Chen, L.-L. Du, W. He, *Nat. Methods* **2020**, *17*, 937.
[4] E. Silvester, B. Vollmer, V. Pražák, D. Vasishtan, E. A. Machala, C. Whittle, S. Black, J. Bath, A. J. Turberfield, K. Grünewald, L. A. Baker, *Cell* **2021**, *184*, 1110.
[5] I. Orlov, A. Schertel, G. Zuber, B. Klaholz, R. Drillien, E. Weiss, P. Schultz, D. Spehner, *Sci. Rep.* **2015**, *5*, 8324.
[6] P. D. Jadzinsky, G. Calero, C. J. Ackerson, D. A. Bushnell, R. D. Kornberg, *Science* **2007**, *318*, 430.
[7] Y. Levi-Kalisman, P. D. Jadzinsky, N. Kalisman, H. Tsunoyama, T. Tsukuda, D. A. Bushnell, R. D. Kornberg, *J. Am. Chem. Soc.* **2011**, *133*, 2976.
[8] C. J. Ackerson, P. D. Jadzinsky, J. Z. Sexton, D. A. Bushnell, R. D. Kornberg, *Bioconjug. Chem.* **2010**, *21*, 214.
[9] C. J. Ackerson, P. D. Jadzinsky, G. J. Jensen, R. D. Kornberg, *J. Am. Chem. Soc.* **2006**, *128*, 2635.
[10] C. L. Heinecke, T. W. Ni, S. Malola, V. Mäkinen, O. A. Wong, H. Häkkinen, C. J. Ackerson, *J. Am. Chem. Soc.* **2012**, *134*, 13316.
[11] V. Marjomaki, T. Lahtinen, M. Martikainen, J. Koivisto, S. Malola, K. Salorinne, M. Pettersson, H. Häkkinen, *Proc. Natl. Acad. Sci. USA* **2014**, *111*, 1277.
[12] M. Martikainen, K. Salorinne, T. Lahtinen, S. Malola, P. Permi, H. Häkkinen, V. Marjomäki, *Nanoscale* **2015**, *7*, 17457.
[13] V. Postupalenko, D. Desplancq, I. Orlov, Y. Arntz, D. Spehner, Y. Mely, B. P. Klaholz, P. Schultz, E. Weiss, G. Zuber, *Angew. Chem. Int. Ed. Engl.* **2015**, *54*, 10583.
[14] M. Azubel, S. D. Carter, J. Weiszmann, J. Zhang, G. J. Jensen, Y. Li, R. D. Kornberg, *Elife* **2019**, *8*, 43146.
[15] D. Desplancq, N. Groysbeck, M. Chiper, E. Weiss, B. Frisch, J.-M. Strub, S. Cianferani, S. Zafeiratos, E. Moeglin, X. Holy, A. L. Favier, S. De Carlo, P. Schultz, D. Spehner, G. Zuber, *ACS Appl. Nano Mater.* **2018**, *1*, 4236.
[16] R. Lévy, N. T. K. Thanh, R. C. Doty, I. Hussain, R. J. Nichols, D. J. Schiffrin, M. Brust, D. G. Fernig, *J. Am. Chem. Soc.* **2004**, *126*, 10076.
[17] A. A. Sousa, J. T. Morgan, P. H. Brown, A. Adams, M. P. S. Jayasekara, G. Zhang, C. J. Ackerson, M. J. Kruhlak, R. D. Leapman, *Small* **2012**, *8*, 2277.
[18] D. Kalderon, B. L. Roberts, W. D. Richardson, A. E. Smith, *Cell* **1984**, *39*, 499.
[19] W. He, M. S. Ladinsky, K. E. Huey-Tubman, G. J. Jensen, J. R. McIntosh, P. J. Bjorkman, *Nature* **2008**, *455*, 542.
[20] L. Boselli, E. Polo, V. Castagnola, K. A. Dawson, *Angew. Chem.* **2017**, *129*, 4279.
[21] J. F. Hainfeld, F. R. Furuya, *J. Histochem. Cytochem.* **1992**, *40*, 177.
[22] C. D. Walkey, J. B. Olsen, F. Song, R. Liu, H. Guo, D. W. H. Olsen, Y. Cohen, A. Emili, W. C. W. Chan, *ACS Nano* **2014**, *8*, 2439.
[23] K. Luby-Phelps, *Int. Rev. Cytol.* **2000**, *192*, 189.
[24] M. Chiper, K. Niederreither, G. Zuber, *Adv. Healthcare Mater.* **2018**, *7*, 1701040.
[25] V. Sokolova, G. Nzou, S. B. van der Meer, T. Ruks, M. Heggen, K. Loza, N. Hagemann, F. Murke, B. Giebel, D. M. Hermann, A. J. Atala, M. Epple, *Acta Biomater.* **2020**, *111*, 349.
[26] V. Sokolova, J.-F. Ebel, S. Kollenda, K. Klein, B. Kruse, C. Veltkamp, C. M. Lange, A. M. Westendorf, M. Epple, *Small* **2022**, *18*, e2201167.
[27] N. Wolff, S. Kollenda, K. Klein, K. Loza, M. Heggen, L. Brochhagen, O. Witzke, A. Krawczyk, I. Hilger, M. Epple, *Nanoscale Adv.* **2022**, *4*, 4502.
[28] J. Y. Wong, T. L. Kuhl, J. N. Israelachvili, N. Mullah, S. Zalipsky, *Science* **1997**, *275*, 820.
[29] Q. Xu, L. M. Ensign, N. J. Boylan, A. Schön, X. Gong, J.-C. Yang, N. W. Lamb, S. Cai, T. Yu, E. Freire, J. Hanes, *ACS Nano* **2015**, *9*, 9217.
[30] N. Groysbeck, A. Stoessel, M. Donzeau, E. C. da Silva, M. Lehmann, J.-M. Strub, S. Cianferani, K. Dembélé, G. Zuber, *Nanotechnology* **2019**, *30*, 184005.
[31] G. L. Ellman, *Arch. Biochem. Biophys.* **1959**, *82*, 70.

[32] E. Oh, J. B. Delehanty, K. E. Sapsford, K. Susumu, R. Goswami, J. B. Blanco-Canosa, P. E. Dawson, J. Granek, M. Shoff, Q. Zhang, P. L. Goering, A. Huston, I. L. Medintz, *ACS Nano* **2011**, *5*, 6434.
[33] X. Liu, M. Atwater, J. Wang, Q. Huo, *Colloids Surf. B Biointerfaces* **2007**, *58*, 3.
[34] G. Creusat, J.-S. Thomann, A. Maglott, B. Pons, M. Dontenwill, E. Guérin, B. Frisch, G. Zuber, *J. Control Release* **2012**, *157*, 418.
[35] R. Lévy, U. Shaheen, Y. Cesbron, V. Sée, *Nano Rev.* **2010**, *1*, 4889.
[36] D. Drescher, T. Büchner, P. Schrade, H. Traub, S. Werner, P. Guttmann, S. Bachmann, J. Kneipp, *ACS Nano* **2021**, *15*, 14838.
[37] S. Pinel, E. Aman, F. Erblang, J. Dietrich, B. Frisch, J. Sirman, A. Kichler, A.-P. Sibler, M. Dontenwill, F. Schaffner, G. Zuber, *J. Controlled Release* **2014**, *182*, 1.
[38] J. B. Gossart, E. Pascal, F. Meyer, E. Heuillard, M. Gonçalves, F. Gossé, E. Robinet, B. Frisch, C. Seguin, G. Zuber, *Met. Sustainability* **2017**, *1*, 1700013.
[39] J. A. Kim, K. Cho, M. S. Shin, W. G. Lee, N. Jung, C. Chung, J. K. Chang, *Biosens. Bioelectron.* **2008**, *23*, 1353.
[40] G. Freund, A.-P. Sibler, D. Desplancq, M. Oulad-Abdelghani, M. Vigneron, J. Gannon, M. H. Van Regenmortel, E. Weiss, *mAbs* **2014**, *5*, 518.
[41] S. C. Ng, D. Görlich, *Nat. Commun.* **2022**, *13*, 6172.
[42] D. Mohr, S. Frey, T. Fischer, D. Görlich, T. Güttler, *EMBO J.* **2009**, *28*, 2541.
[43] K. Ribbeck, D. Gorlich, *EMBO J.* **2001**, *20*, 1320.
[44] G. Chen, X. Deng, *Bio Protoc.* **2018**, *8*, 2994.
[45] A. P. Schuller, M. Wojtynek, D. Mankus, M. Tatli, R. Kronenberg-Tenga, S. G. Regmi, P. V. Dip, A. K. R. Lytton-Jean, E. J. Brignole, M. Dasso, K. Weis, O. Medalia, T. U. Schwartz, *Nature* **2021**, *598*, 667.
[46] T. V. Hoang, C. Kizilyaprak, D. Spehner, B. M. Humbel, P. Schultz, *J. Struct. Biol.* **2017**, *197*, 123.
[47] J. Schindelin, I. Arganda-Carreras, E. Frise, V. Kaynig, M. Longair, T. Pietzsch, S. Preibisch, C. Rueden, S. Saalfeld, B. Schmid, J.-Y. Tinevez, D. J. White, V. Hartenstein, K. Eliceiri, P. Tomancak, A. Cardona, *Nat. Methods* **2012**, *9*, 676.
[48] R. W. Burry, D. D. Vandre, D. M. Hayes, *J. Histochem. Cytochem.* **1992**, *40*, 1849.

